
ARTICLE

CFD analysis of thermal radiation effects on large containment CIGMA vessel with Weighted Sum of Gray Gases (WSGG) model

Ari Hamdani ^{a*}, Shu Soma ^a, Satoshi Abe ^b and Yasuteru Sibamoto ^a

^a Japan Atomic Energy Agency, 2-4 Shirakata, Tokai-mura, Naka-gun, Ibaraki 319-1195, Japan; ^b Nuclear Regulation Authority, 1-9-9 Roppongi, Minato-ku, Tokyo 106-8450, Japan

This paper presents the experimental study and computational fluid dynamics (CFD) analysis on the effect of thermal radiation in the humid atmosphere inside the containment vessel. The experiment was conducted in the Containment InteGral effects Measurement Apparatus (CIGMA) facility at Japan Atomic Energy Agency (JAEA). The numerical analysis was carried out using the open-source CFD code OpenFOAM®. The initial gas condition inside the CIGMA containment consists of three gases, helium, air, and water vapor, at room temperature 30 °C and a pressure of 1 atm. Initial helium stratification was located 6 m above the bottom vessel, and its molar fraction was 55 %. The initial water vapor molar fraction was set to 0.1 % to minimize the thermal radiation absorption by the water molecule. Pure helium was injected through a nozzle from the top, leading to increased vessel pressure and a corresponding rise in gas temperature. The numerical validation at low water vapor, i.e., 0.1% H₂O, was performed by comparing the transient profile of pressure, gas molar fraction, and temperature with the experimental data. A Weighted Sum of Gray Gases (WSGG) model was implemented in the OpenFOAM® solver. The numerical results showed a reasonable agreement compared to the experimental data. In addition, the numerical simulation with various water vapor mass fractions, i.e., 0.0%, 0.1%, 0.3%, 0.5%, and 60%, was performed to analyze the effect of humidity on the radiative heat transfer. The predicted temperature was overestimated when the numerical model neglected thermal radiation. Therefore, it indicated that thermal radiation should be considered when modeling the containment thermohydraulic.

Keywords: *computational fluid dynamics; thermohydraulic; containment; thermal radiation; CIGMA; OpenFOAM*

Nomenclature		Greek letters	
D	Diffusion coefficient [m ² /s]	α	Thermal diffusivity [m ² /s]
G	Total incident radiation [W/m ²]	ρ	Density [kg/m ³]
g	Acceleration due to gravity [m/s ²]	ν	Kinematic viscosity [m ² /s]
h	Enthalpy [J/kg]	λ	Thermal conductivity [W/(m·K)]
p	Pressure [Pa]	σ	Stefan-Boltzmann constant [5.67×10 ⁻⁸ W/m ² /K ⁴]
Pr	Prandtl number	∇	Nabla-operator
q_r''	Radiative heat flux [W/m ²]	Subscripts	
S	Source term	eff	Effective
Sc	Schmidt number	t	Turbulent
T	Temperature [K]	k	Species index
t	Time [s]		
u	Velocity [m/s]		

1. Introduction

During a postulated nuclear accident, a vast amount of steam and hydrogen might be released inside the containment vessel. Accordingly, the investigations on gas transport and mixing in a containment vessel have become an

important research topic to determine hydrogen-related risks [1]. Formerly, several national and international projects related to the hydrogen-related risks in nuclear containment vessels had been studied in different research facilities [2-4]. Those projects' experimental databases are essential for assessing the numerical modeling of nuclear reactor safety. Previous numerical computational fluid dynamics (CFD) analysis on the erosion of a stratified containment atmosphere by a vertical jet showed that

*Corresponding author.

E-mail: ari.hamdani@jaea.go.jp (A. Hamdani).

considering radiative heat transfer in the numerical model led to an improvement in the simulation results [5,6]. Therefore, it is very important to study the radiative heat transfer inside the containment vessel since steam has a large absorption coefficient in the infrared spectrum. Furthermore, the radiative heat transfer in the containment thermohydraulic as a separate test needs to be further investigated. Recently, under the framework of the OECD/NEA HYMERES-2 project, an experimental study on containment thermohydraulic phenomena which have safety relevance was performed in the PANDA facility at Paul Scherer Institute (PSI). One of the experiment series, i.e., H2P2, focused on the effects of radiative heat transfer on the thermal evolution of the containment atmosphere [7, 8].

Numerical CFD modeling of radiative heat transfer inside the containment vessel is challenging since the presence of participating medium. Subject to the presence of non-gray gas, i.e., steam/H₂O, the emission and absorption coefficient of H₂O in the radiative transport equations (RTE) depends on the wavelength. Thus, steam is the main contributor to radiative heat transfer in the containment thermohydraulic. Typically, all spectral bands of H₂O are required to resolve RTE (as described by a Line-by-Line model). The Line-by-line (LBL) model can deal with local variations in the concentration of the participating gas species [9]. However, the LBL model needs integration over the entire spectrum, which is computationally expensive for most engineering applications. As an alternative to evaluating the absorption/emission coefficient, the weighted sum of grey gases (WSGG) model was proposed by [10]. The WSGG model is a global spectral model in which the radiation spectrum is represented by a small set of gray gases with uniform absorption coefficients plus transparent windows [11]. The WSGG model is regarded as a reasonable compromise between the oversimplified grey gas model and a narrow band type model that considers particular absorption bands [12].

In this work, the thermal radiation experiment that is similar to one of the H2P2 series, i.e., H2P2_1_2, was performed in the CIGMA facility at Japan Atomic Energy

Agency (JAEA). Later, the experimental data was used to validate the numerical CFD model. A 3D numerical CFD simulation was carried out using the open-source CFD code OpenFOAM[®]. The CFD simulation was performed to analyze the detailed effect of thermal radiation inside a large containment vessel. A Weighted Sum of Gray Gases (WSGG) model was implemented in the OpenFOAM[®] solver. The numerical validation at low water vapor, i.e., 0.1% H₂O, was done by comparing the transient profile of pressure, gas molar fraction, and temperature with the experimental data. In addition, the numerical model with various water vapor molar fractions, i.e., 0.0%, 0.1%, 0.3%, 0.5%, and 60%, was simulated to analyze the effect of humidity on the radiative heat transfer. The pressure history, temperature, and molar fraction variations of water vapor are quantified and discussed.

2. Methodology

2.1. Experiment facility and initial boundary conditions

Figure 1(a) shows the drawing of the CIGMA experimental facility at the Japan Atomic Energy Agency (JAEA). CIGMA containment vessel is a large cylindrical stainless steel with an inner diameter of the main cylindrical part of 2.5 m and an overall height of 11 m. The whole vessel is thermally isolated using rock-wool mats covered by reinforced wire mesh to avoid significant heat loss. The temperature and pressure boundary of the containment vessel can withstand up to 300 °C and 1.5 MPa. The test section of CIGMA has many thermocouples (TCs), i.e., 650 TCs and capillary tubes (CTs), i.e., 100 CTs to measure the temperature and gas concentration. A K-type thermocouple is used to measure both gas and wall temperature. A quadrupole mass spectrometer (QMS) with sampling tubes and a multiport rotating valve is used to measure gas concentrations. Please refer to our previous publications [13][14][15] for a more detailed description of the CIGMA facility.

The thermal radiation experiment similar to the H2P2 series [16] was conducted in the CIGMA facility. **Figure 1(b)** depicts the initial gas condition inside the containment that consists of three gases, helium, air, and water vapor,

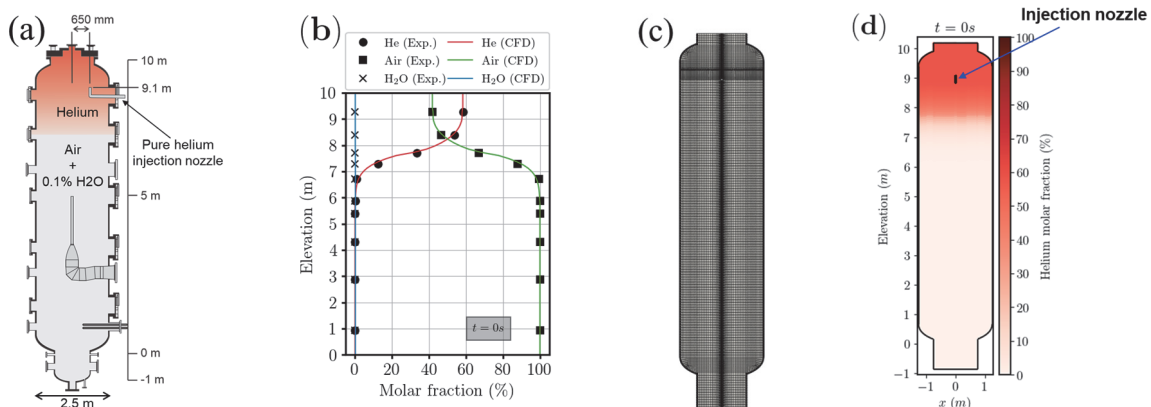


Figure 1. (a) CIGMA experiment facility, (b) Initial condition of gases, (c) Numerical mesh, (d) Contour plot of helium molar fraction and the location of the injection nozzle in the numerical model.

Table 1. Experimental conditions.

	Parameters	Value
Initial conditions before compression	Pressure	1 atm
	Temperature	30 °C
	H ₂ O	0.1 %
	Helium at the top vessel	55 %
Compression	A mass flow rate of pure helium injection	5.6 g/s
	Injection temperature	30 °C
	Injection time	1200 s

at room temperature of 30°C and a pressure of 1 atm. Initial helium stratification was located 6 m above the bottom vessel, and its molar fraction was 55%. The initial water vapor molar fraction was set to 0.1%. Pure helium was injected through a nozzle with a mass flow rate of 5.6 g/s from the top for 1200 seconds. The compression process leads to increased vessel pressure and a corresponding rise in gas temperature. The detailed experimental conditions are described in **Table 1**.

The computational domain was discretized using a fully hexahedral mesh, employing the O-grid technique as depicted in **Figure 1(c)**. The radial direction features a minimum cell size of 1.3 mm, while cells are more refined near the nozzle exit and center due to larger gradients (for example, velocity) within these regions. A mesh convergence study was conducted in our previous work, establishing that an average cell size of 50 mm × 50 mm × 75 mm in the x, y, and z directions respectively is the minimum prerequisite for grid convergence in the bulk region. The computational model comprises a total of 848,130 cells, with an average non-orthogonality of 4 and a maximum aspect ratio of 70, ensuring a fine and accurate representation of the physical phenomena involved. The initial conditions of the CFD model are set according to the experimental data, as shown in Figure (b). The computational domain was simplified by neglecting solid stainless-steel walls and internal structures, e.g., main nozzle injection. In addition, the helium injection nozzle was located in the center for simplification during the meshing process, and the injection line was not modeled, as shown in **Figure 1(d)**.

2.2. Numerical modeling and procedure

The fireFOAM solver is employed in the present analysis. It is an open-source software package that was initially developed and maintained by FM Global based on the platform OpenFOAM®. The solver uses fully compressible flow formulation and solves the Navier-Stokes equations using Favre-filtered quantities. The Reynolds-averaged equations for continuity, momentum, mass transport, and energy are described below. The bracket [] denotes the Reynolds-averaging operation, and the angle bracket <> expresses the Favre density averaging.

$$\frac{\partial \langle \rho \rangle}{\partial t} + \frac{\partial \langle \rho \rangle [u_i]}{\partial x_i} = 0 \quad (1)$$

$$\begin{aligned} & \frac{\partial \langle \rho \rangle [u_i]}{\partial t} + \frac{\partial \langle \rho \rangle [u_i] [u_j]}{\partial x_j} \\ &= -\frac{\partial \langle p \rangle}{\partial x_i} + \frac{\partial}{\partial x_j} \left\{ \mu \left(\frac{\partial [u_i]}{\partial x_j} + \frac{\partial [u_j]}{\partial x_i} - \frac{2}{3} \frac{\partial [u_k]}{\partial x_k} \delta_{ij} \right) - \langle \rho \rangle [u'_i u'_j] \right\} \\ & \quad + \langle \rho \rangle g_i \end{aligned} \quad (2)$$

$$\frac{\partial \langle \rho \rangle [Y_k]}{\partial t} + \frac{\partial \langle \rho \rangle [u_i] [Y_k]}{\partial x_j} = \frac{\partial}{\partial x_i} \left(\langle \rho \rangle D_k \frac{\partial [Y_k]}{\partial x_i} - \langle \rho \rangle [u'_i Y'_k] \right) \quad (3)$$

$$\begin{aligned} & \frac{\partial \langle \rho \rangle [h]}{\partial t} + \frac{\partial \langle \rho \rangle [u_i] [h]}{\partial x_i} \\ &= \frac{\partial}{\partial x_i} \left\{ \langle \rho \rangle \alpha \frac{\partial [h]}{\partial x_i} + \sum_{k=1}^N \langle p \rangle (D_k - \alpha) [h_k] \frac{\partial [Y_k]}{\partial x_i} - \langle \rho \rangle [u'_i h'] \right\} \\ & \quad + \frac{\partial \langle p \rangle}{\partial t} - \nabla \cdot \langle \dot{q}'_r \rangle \end{aligned} \quad (4)$$

The terms with a fluctuation component in Eqs. (2), (3), and (4) are expressed with the prime mark and modeled with a simple gradient diffusion hypothesis (SGDH) as follows

$$\langle \rho \rangle [u'_i u'_j] = -\mu_t \left(\frac{\partial [u_i]}{\partial x_j} + \frac{\partial [u_j]}{\partial x_i} - \frac{2}{3} \frac{\partial [u_k]}{\partial x_k} \delta_{ij} \right) + \frac{2}{3} \langle \rho \rangle k \delta_{ij} \quad (5)$$

$$\langle \rho \rangle [u'_i Y'_k] = -\langle \rho \rangle D_t \frac{\partial [Y_k]}{\partial x_i} = -\langle \rho \rangle \frac{v_t}{Sc_t} \frac{\partial [Y_k]}{\partial x_i} \quad (6)$$

$$\langle \rho \rangle [u'_i h'] = -\langle \rho \rangle \alpha_t \frac{\partial [h]}{\partial x_i} + \sum_{k=1}^N \langle p \rangle (D_t - \alpha_t) [h_k] \frac{\partial [Y_k]}{\partial x_i} \quad (7)$$

The radiative heat flux in Eq. 4 is calculated as:

$$\nabla \cdot \langle \dot{q}'_r \rangle = \langle a \rangle (4\sigma [T]^4 - [G]) \quad (8)$$

Where ρ is density, x_i and u_i denote the distance and flow velocity in the i -direction, $k = 1, 2, \dots, N$ and N is the number of total species, Y_k is the mass fraction of gas species k and D_k is the molecular diffusivity of the mass fraction of species k in the mixture, ν_t , α_t , D_t are turbulent/eddy viscosity, turbulent thermal diffusivity, and turbulent mass diffusivity. Turbulent/eddy viscosity ν_t is calculated with the formulation according to k - ω SST turbulence model. σ is the Stefan-Boltzmann constant, and G

is the total irradiance. A unity Lewis number assumption is employed in the present model. Thus, the turbulent Prandtl number Pr_t was assumed to equal the turbulent Schmidt number Sc_t .

The finite volume discrete ordinates model (fvDOM) is used to solve the radiative heat transfer equation. The WSGG model is linked to the FireFOAM solver and is modeled using a modified fvDOM developed by [17]. The modified fvDOM allows for banded or non-grey solutions of the radiative transfer equation (RTE). In the present analysis, the parametric database of [18] was used because it is reasonably accurate and simpler than another database.

The Reynolds-averaged Navier-Stokes equations (RANS) model is employed in the present analysis. The numerical discretization of the governing equations is second-order accurate in time and space. The gradient terms are discretized by the central differencing scheme, and the divergence terms are discretized by the linear scheme with the total variation diminishing (TVD) scheme. The temporal term is discretized by the implicit backward Euler scheme. For the Radiative Transfer Equation (RTE) solution, 60 solid angles are used for angular discretization. The PIMPLE algorithm, which combines the PISO (pressure implicit with splitting of operator) and SIMPLE (semi-implicit method for pressure linked equations) algorithms, is used for coupling between velocity and pressure fields. The time step is adjusted to $\Delta t = 0.005$ s during the transient simulations, corresponding to the Courant number less than 1.

2.3. Validation of the numerical model

The numerical validation at low water vapor, i.e., 0.1%

H_2O , was performed by comparing the transient profile of pressure, gas temperature, and molar fraction with the experimental data, as shown in **Figure 2**. Figure 2 (a) shows the pressure comparison between experiment and numerical result during the helium compression for 1200 s. The black line represents the experimental data, and the red line represents the numerical result. The numerical prediction on pressure shows a similar trend as the experimental data. The helium compression process leads to increased vessel pressure. However, the predicted pressure is overestimated compared to the experiment. The gas temperature at the end of the compression phase for the experiment and CFD simulation are presented in Figures 2(b) and 2(c), respectively.

As expected, the helium compression process increases gas temperature below the helium layer. The small black dots in Figures 2(b) depict the location of the thermocouples in the CIGMA facility. The CFD result on the pressure rise shows qualitative agreement with the experiment. However, quantitatively, the CFD result on the gas temperature rise exceeds the experimental value. At $t = 1200$ s, the maximum gas temperature difference between CFD and the experiment reaches 30°C . This large temperature difference is mainly caused by the boundary condition at the wall surface. In the present model, the thermal radiation absorption by the wall surface is underestimated. In fact, the CIGMA wall surface was black painted, and it was confirmed in the experimental data that the inner wall surface temperature slightly increased during the compression phase. It suggested that the wall surface also absorbed the thermal radiation. The transient evolution of helium gas at the vessel center axis is presented in **Figure 3**. As we can see in Figures 3, the

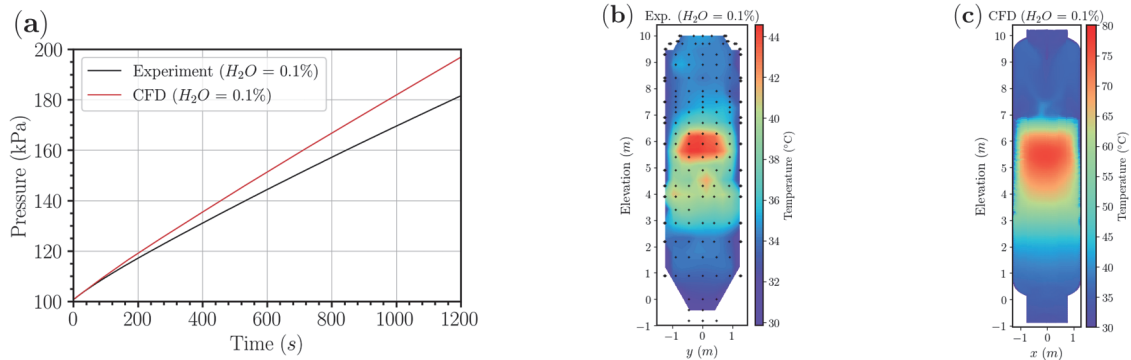


Figure 2. Comparison of CFD model with the experimental data (a) Validation of pressure history, (b) Experimental temperature contour plot at $t = 1230$ s, (c) Numerical temperature contour plot at $t = 1200$ s.

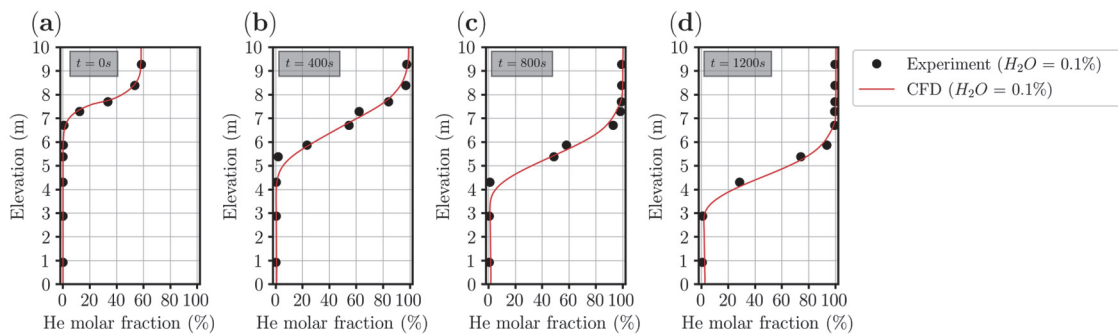


Figure 3. Comparison of predicted helium profile with the experimental data at (a) $t = 0$ s, (b) $t = 400$ s, (c) $t = 800$ s, (d) $t = 1200$ s.

predicted helium molar fraction agrees very well with the experimental data. At $t = 0$ s, the maximum helium molar fraction in the top vessel is around 60%. Later, at $t = 400$ s, the helium molar fraction in the top vessel becomes 98% because pure helium is injected from the top vessel. At $t = 800$ s, we can observe that pure helium stratification moves downward. Finally, at the end of compression, i.e., $t = 1200$ s, the helium molar fraction reaches 100% above the elevation $z > 7$ m, followed by a steep gradient between elevation $3 \text{ m} < z < 7 \text{ m}$.

3. Results and discussion

3.1. Effect of initial H₂O molar fraction

The numerical simulation with various water vapor molar fractions, i.e., 0.0%, 0.1%, 0.3%, 0.5%, and 60% H₂O, was performed to analyze the effect of humidity on the radiative heat transfer. A large amount of water vapor, i.e., 60%, was selected because the steam content in the gas mixture might reach 60% or more during a severe nuclear accident [19]. Thus, in the case of 60% H₂O, we expected that steam's heat absorption might play a dominant role in the radiative heat transfer.

Figure 4 depicts the pressure history for various water vapor. At $t = 1200$ s, we can observe that the pressure with 60% H₂O is slightly lower than other water vapor molar fractions. It suggests that the radiative heat transfer does not significantly affect the pressure rise inside the containment vessel.

Figure 5(a) depicts the helium molar fraction profile at the center axis for all various water vapor at the end of the compression phase, $t = 1200$ s. The pure helium injection from the top vessel caused the helium molar fraction at the top vessel to be 100 %, followed by a steep gradient

between elevation $3 \text{ m} < z < 7 \text{ m}$. There are no significant differences in the helium molar fraction profile for all various water vapors. It also suggests that the effect of radiative heat transfer on the gas mixture molar fraction inside the vessel is negligibly small. **Figure 5(b)** depicts the temperature profile at the vessel center axis for all various water vapor at the end of the compression phase, $t = 1200$ s. We can clearly observe that the gas temperature, at $t = 1200$ s, varies depending on the initial water vapor. Also, as expected, the highest gas temperature is observed at 0.0% H₂O, and the lowest gas temperature is observed at 60% H₂O. **Figure 5(c)** depicts the excess temperature where the temperature is normalized with the average initial temperature \bar{T}_0 at the beginning of compression. The maximum excess temperature at 0.0%, 0.1%, 0.3%, 0.5%, and 60% H₂O is around 60°C, 44°C, 35°C, 32°C, and 12°C, respectively. It indicates that the rise of gas temperature highly depends on the initial water vapor. Therefore, the thermal absorption by water molecules is very important in evaluating the radiative heat transfer inside the containment vessel.

3.2. Effect of thermal radiation

The thermal radiation effect is evaluated by numerical simulation at water vapor molar fractions of 0.1% and 60%, with and without the radiation model. The initial and boundary conditions are identical for both with the radiation model (hereinafter abbreviated as *rad*) and without the radiation model (hereinafter abbreviated as *noRad*). The main difference between those models is that the source term radiative heat flux was not included in the *noRad* model. Thus, in the *noRad* model, it is assumed that the radiation absorption by water molecules is not

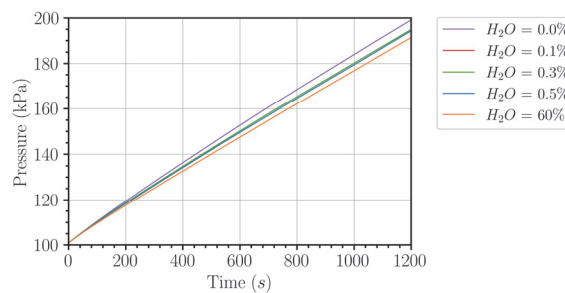


Figure 4. Pressure history for various water vapor.

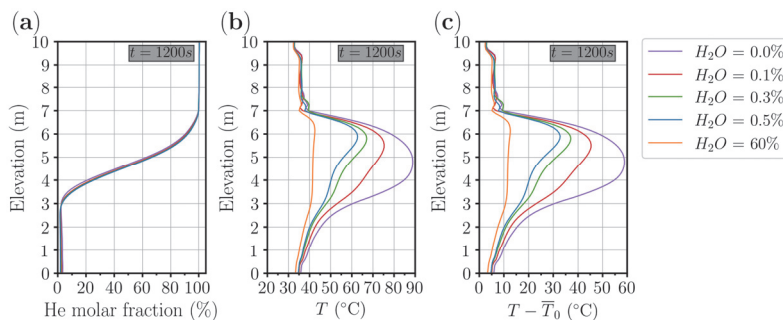


Figure 5. (a) Helium molar fraction profile at $t = 1200$ s, (b) Temperature profile at $t = 1200$ s, (c) Excess temperature profile at $t = 1200$ s.

considered. **Figure 6** depicts the pressure history of both *rad* and *noRad* models. At $t = 1200$ s, the pressure of *noRad* model is slightly higher than *rad* model. **Figure 7(a)** and **7(b)** depict the gas temperature profile of both water molar fraction 0.1% and 60% H_2O with *rad* and *noRad* models. We can observe in Figure 7(a) that the maximum temperature with *noRad* model at 0.1% H_2O is $15^\circ C$ higher than the *rad* model. Meanwhile, in Figure 7(b), the maximum temperature with *noRad* model at 60% H_2O is $40^\circ C$ higher than the *rad* model. A significant temperature overestimation is observed when the water vapor content in the gas mixture is large, e.g., $H_2O = 60\%$. It indicates that neglecting radiative heat transfer in the numerical model leads to overestimating temperature.

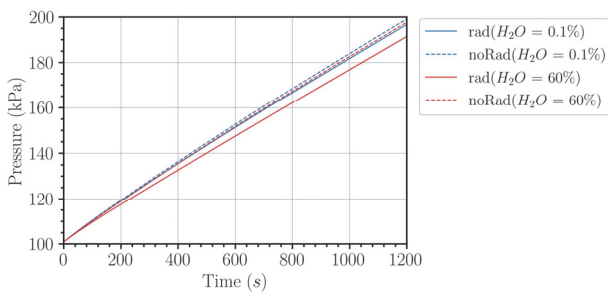


Figure 6. Pressure history of both radiation (*rad*) and non-radiation (*noRad*) model.

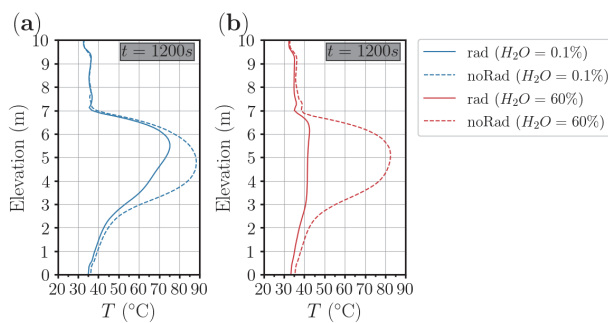


Figure 7. (a) Temperature profile with $H_2O = 0.1\%$ at $t = 1200$ s, (b) Temperature profile with $H_2O = 60\%$ at $t = 1200$ s.

4. Conclusion

A separate test on radiative heat transfer has been conducted in the CIGMA containment vessel at JAEA. In addition, a numerical CFD simulation using the RANS approach has been performed to evaluate the effect of thermal radiation inside the containment vessel. The main conclusions of the study are summarized as follows:

1. CFD results on the pressure history with the WSGG model showed a reasonable agreement with the experiment. However, the predicted gas temperature was still overestimated since the thermal radiation absorption by the wall was underestimated in the present CFD model.
2. The variation of water vapor molar fractions in the gas mixture had a small effect on the pressure rise

and gas mixture composition during the compression phase. However, the variation of water vapor molar fractions in the gas mixture significantly affects the gas temperature. The temperature rise on the gas mixture decreased as the water vapor molar fraction increased.

3. It was confirmed that neglecting radiative heat transfer in the numerical model led to a significant overestimation of gas temperature. Furthermore, the maximum temperature difference between the model with and without radiation was even more remarkable as the water vapor molar fraction inside the containment vessel increased.

Acknowledgements

The construction of the CIGMA facility and the experiments in this work were conducted under the auspices of the Nuclear Regulation Authority (NRA), Japan. The authors acknowledge our colleagues, who provided the expertise that greatly assisted the investigation. In addition, the authors would like to show our gratitude to all staff and Nuclear Engineering Co., Ltd. members who were involved and conducted the CIGMA experiments.

References

- [1] S. Gupta, Experimental investigations relevant for hydrogen and fission product issues raised by the Fukushima accident, *Nuclear Engineering and Technology* 47 (2015), pp. 11-25.
- [2] J. Malet, E. Porcheron and J. Vendel, OECD International Standard Problem ISP-47 on containment thermal-hydraulics - Conclusions of the TOSQAN part, in *Nuclear Engineering and Design* 240 (2010), pp. 3209-3220.
- [3] OECD/NEA/CSNI, OECD / SETH-2 Project PANDA and MISTRA Experiments Final Summary Report - Investigation of Key Issues for the Simulation of Thermal- hydraulic Conditions in Water Reactor Containment, *NEA/CSNI/R(2012)5, Organisation for Economic Co-operation and Development/Nuclear Energy Agency Committee on the Safety of Nuclear Installations*, April, 2012.
- [4] S. Gupta, et al., THAI test facility for experimental research on hydrogen and fission product behaviour in light water reactor containments, *Nuclear Engineering and Design* 294 (2015), pp. 183-201.
- [5] M. Andreani, et al., Synthesis of a CFD benchmark exercise based on a test in the PANDA facility addressing the stratification erosion by a vertical jet in presence of a flow obstruction, *Nuclear Engineering and Design*, 354 (2019), p. 110177.
- [6] X. Liu, S. Kelm, M. Kampili, G.V. Kumar and H.-J. Allelein, Monte Carlo method with SNBCK nongray gas model for thermal radiation in containment flows, *Nuclear Engineering and Design* 390 (2022), p. 111689.
- [7] D. Paladino, R. Kapulla, S. Paranjape, S. Suter and M. Andreani, PANDA experiments within the OECD/NEA HYMERES-2 project on containment hydrogen distribution, thermal radiation and suppression

- pool phenomena, *Nuclear Engineering and Design* 392 (2022).
- [8] R. Kapulla, S. Paranjape, U. Doll, E. Kirkby and D. Paladino, Experimental assessment of thermal radiation effects on containment atmospheres with varying steam content, *Nuclear Engineering and Technology* 54 (2022), pp. 4348-4358.
- [9] F.R. Centeno, R. Brittes, L.G.P. Rodrigues, F.R. Coelho and F.H.R. França, Evaluation of the WSGG model against line-by-line calculation of thermal radiation in a non-gray sooting medium representing an axisymmetric laminar jet flame, *International Journal of Heat and Mass Transfer* 124 (2018), pp. 475-483.
- [10] H.C. Hottel and A.F. Sarofim, *Radiative Transfer* (1967), New York, NY: McGraw-Hill.
- [11] M.F. Modest, *Radiative Heat Transfer* (2013). Elsevier.
- [12] C.J. Wang, J.X. Wen, Z.B. Chen and S. Dembele, Predicting radiative characteristics of hydrogen and hydrogen/methane jet fires using FireFOAM, *International Journal of Hydrogen Energy* 39 (2014), pp. 20560-20569.
- [13] M. Ishigaki, S. Abe, Y. Sibamoto and T. Yonomoto, Experimental investigation of density stratification behavior during outer surface cooling of a containment vessel with the CIGMA facility, *Nuclear Engineering and Design* 367 (2020), p. 110790.
- [14] S. Abe, A. Hamdani, M. Ishigaki and Y. Sibamoto, Experimental investigation of natural convection and gas mixing behaviors driven by outer surface cooling with and without density stratification consisting of an air-helium gas mixture in a large-scale enclosed vessel, *Annals of Nuclear Energy* 166 (2022), p. 108791.
- [15] A. Hamdani, S. Abe, M. Ishigaki, Y. Sibamoto and T. Yonomoto, CFD analysis on stratification dissolution and breakup of the air-helium gas mixture by natural convection in a large-scale enclosed vessel, *Progress in Nuclear Energy*, 153 (2022), p. 104415.
- [16] R. Kapulla, S. Paranjape, U. Doll, E. Kirkby and D. Paladino, Experimental assessment of thermal radiation effects on containment atmospheres with varying steam content, *Nuclear Engineering and Technology* 54 (2022), pp. 4348-4358.
- [17] I. Sikic, S. Dembele and J. Wen, Non-grey radiative heat transfer modelling in LES-CFD simulated methanol pool fires, *Journal of Quantitative Spectroscopy and Radiative Transfer* 234 (2019), pp. 78-89.
- [18] T.F. Smith, Z.F. Shen and J.N. Friedman, Evaluation of coefficients for the weighted sum of gray gases model, *Journal of Heat Transfer* 104 (1982), pp. 602-608.
- [19] J.C. de la Rosa, A. Escrivá, L.E. Herranz, T. Cicero and J.L. Muñoz-Cobo, Review on condensation on the containment structures, *Progress in Nuclear Energy* 51 (2009), pp. 32-66.
-